

High-Performance Unidirectional Manipulation of Microdroplets by Horizontal Vibration on Femtosecond Laser-Induced Slant Microwall Arrays

Dong Wu, Zhen Zhang, Yiyuan Zhang, Yunlong Jiao, Shaojun Jiang, Hao Wu, Chuanzong Li, Chenchu Zhang, Jiawen Li, Yanlei Hu,* Guoqiang Li,* Jiaru Chu, and Lei Jiang*

The high-performance unidirectional manipulation of microdroplets is crucial for many vital applications including water collection and bioanalysis. Among several actuation methods (e.g., electric, magnetic, light, and thermal actuation), mechanical vibration is pollution-free and biocompatible. However, it suffers from limited droplet movement mode, small volume range ($V_{\text{Max}}/V_{\text{Min}} < 3$), and low transport velocity ($\leq 11.5 \text{ mm s}^{-1}$) because the droplet motion is a sliding state caused by the vertical vibration on the asymmetric hydrophobic microstructures. Here, an alternative strategy is proposed—horizontal vibration for multimode (rolling, bouncing/reverse bouncing, converging/diffusing, climbing, 90° turning, and sequential transport), large-volume-range ($V_{\text{Max}}/V_{\text{Min}} \approx 100$), and high-speed ($\approx 22.86 \text{ mm s}^{-1}$) unidirectional microdroplet manipulation, which is ascribed to the rolling state on superhydrophobic slant microwall arrays (SMWAs) fabricated by the one-step femtosecond laser oblique ablation. The unidirectional transport mechanism relies on the variance of viscous resistance induced by the difference of contact area between the microdroplet and the slant microwalls. Furthermore, a circular, curved, and “L”-shaped SMWA is designed and fabricated for droplet motion with particular paths. Finally, sequential transport of large-volume-range droplets and chemical mixing microreaction of water-based droplets are demonstrated on the SMWA, which demonstrates the great potential in the field of microdroplet manipulation.


Microdroplet manipulation has attracted great interest in many fields including water collection,^[1–3] digital microfluidics,^[4–6] precious liquid microreaction,^[7–9] and biomedical analysis.^[10–13] A variety of manipulation strategies with an external energy input were developed, such as electric,^[14] magnetic,^[15] light,^[16] and thermal field.^[17] However, they are hindered by their inherent limitations. For example, the electrowetting-on-dielectric actuates droplet motion through a large contact angle change induced by the electric field, which is often limited by the electrical breakdown of the dielectrics. Magnetic actuation requires the existence of magnetic nanoparticles to respond to external varying magnetic fields, which is detrimental to bioassay and medical analysis. Light actuation utilizes light-induced surface tension difference to drive droplets, which cannot manipulate large droplets at a high speed. Thermal actuation can achieve the directional propulsion of droplets under the Leidenfrost state by

Prof. D. Wu, Y. Zhang, S. Jiang, H. Wu, Prof. J. Li, Prof. Y. Hu, Prof. J. Chu
CAS Key Laboratory of Mechanical Behavior and Design of Materials
Key Laboratory of Precision Scientific Instrumentation of Anhui
Higher Education Institutes
Department of Precision Machinery and Precision Instrumentation
University of Science and Technology of China
Hefei 230027, China
E-mail: huyl@ustc.edu.cn

Z. Zhang
CAS Key Laboratory of Geospace Environment
USTC
Hefei 230026, China

Prof. Y. Jiao
Institute of Tribology
Hefei University of Technology
Hefei 230009, P. R. China

C. Li
School of Instrument Science and Opto-electronics Engineering
Hefei University of Technology
Hefei 230009, P. R. China

 The ORCID identification number(s) for the author(s) of this article can be found under <https://doi.org/10.1002/adma.202005039>.

Prof. C. Zhang
Institute of Industry and Equipment Technology
Hefei University of Technology
Hefei 230009, P. R. China

Prof. G. Li
Key Laboratory of Testing Technology for Manufacturing Process
of Ministry of Education
Southwest University of Science and Technology
Mianyang 621010, China
E-mail: guoqli@swust.edu.cn

Prof. L. Jiang
CAS Key Laboratory of Bio-inspired Materials and Interfacial Sciences
Technical Institute of Physics and Chemistry
Chinese Academy of Sciences
Beijing 100190, China
E-mail: jianglei@iccas.ac.cn

Prof. L. Jiang
Future Technology College
University of Chinese Academy of Sciences
Beijing 100049, China

DOI: 10.1002/adma.202005039

significantly increasing the local temperature of the surface asymmetric microstructures, which is not conducive to biomedical detection and analysis. In addition, a novel strategy for high-velocity and ultralong droplet transport elicited by surface charge density gradient has been reported recently, which is yet not working well in wet conditions due to the potential degradation of surface charge.^[18]

Mechanical vibration is a facile and highly efficient strategy to manipulate droplet motion with some unique advantages.^[19–26]

1) It is robust and durable in contrast to electrowetting, which is easily damaged. 2) There is no cross-contamination because there is no need to dope droplets with special particles. Daniel and Chaudhury^[27,28] et al. demonstrated a drop motion along the wetting gradient by a periodic force. Moreover, they presented a uniformly hydrophobic silicon wafer modified with a self-assembled monolayer of alkyltrichlorosilane, which move the droplet unidirectionally and reversibly by asymmetric inertial force induced by asymmetric lateral vibration. Demirel et al.^[29] first reported an engineered nanofilm composed of an array of poly(p-xylylene) nanorods fabricated by oblique angle polymerization, which realized the unidirectional motion of droplets under vertical vibration. The mechanism lies on the anisotropic wetting behavior based on a pin–release droplet ratchet model. Böhringer et al.^[30] further introduced a texture ratchet—substrates that can controllably propel droplets along the horizontal surface under vertical vibration, which is mainly related to asymmetric pinning forces along the triple contact line. Although great progress has been made, there are still several disadvantages to address. 1) The manipulation capability focused on simple transport modes of droplets with limited volume range at a relative low speed, while some complex modes (rolling, bouncing/reverse bouncing, converging/diffusing, climbing, 90° turning, and sequential transport) are challenging. 2) The surface is not superhydrophobic (85°–150°), and the motion state is sliding. The droplet volume is limited to microliter levels ($\geq 4 \mu\text{L}$) while nanoliter droplets cannot be manipulated effectively. 3) The motion speed of droplets is moderate ($\approx 11.5 \text{ mm s}^{-1}$), and should be further enhanced. 4) The fabrication of the above functional surfaces requires complex preparation processes and chemical treatment. Another interesting thing is that the vibration direction is vertical and the droplet motion is “sliding state.” Thus, our work explores the question of whether there exist new vibration strategies and droplet motion modes, which could substantially enhance the performance of water-based droplet manipulation.

Here we answer this question through reporting an unanticipated phenomenon: The high-performance manipulation of water droplets on slant microwall arrays (SMWA) structures prepared by one-step femtosecond laser oblique ablation (FLOA). We find that on such unique morphologies, the droplets oscillate in situ up and down under vertical vibration, and oscillate in situ left and right under horizontal vibration parallel to the microwall direction (HV_{\parallel}), but transport at a high speed of Videos S1 and S2, Supporting Information, under horizontal vibration perpendicular to the microwall direction (HV_{\perp}) on the SMWA surface. Based on HV_{\perp} , the droplet can move as fast as 22.86 mm s^{-1} in a “rolling state.” Furthermore, the effects of droplet size, excitation intensity, and structure size of the microwalls on droplet transport capacity such as grade-ability

are also studied. The range of droplet volumes can even be expanded to nanoliter levels ($\approx 53 \text{ nL}$), which is much smaller than that by previous mechanical methods. In addition, it is clarified that the mechanical mechanism lies in the variance of viscous resistance caused by the difference of contact area between droplet and slant microwalls. Furthermore, some particular microdroplet motions (convergence/diffusion, climbing, and 90° turning) are realized by designing the circular, curved, and “L”-shaped SMWA. Finally, sequential transport of large-volume-range droplets and chemical mixing microreaction of water-based droplets are demonstrated on the horizontally-vibrating SMWA. Compared with the present works, SMWA manifests the great potential applications in the field of microdroplet manipulation.

Figure 1a shows that a kind of bioinspired asymmetric SMWA is designed and fabricated by a top-down FLOA technique in Figures S1 and S2, Supporting Information. The FLOA involves oblique laser focusing and horizontal motion of the sample using the commercial XY scanning platform (see Experimental Section) without compositional substances change in Figure S3, Supporting Information. This distinct SMWA can derive the unidirectional transport capability of microdroplets under horizontal vibration. Figure 1b shows the cross-section of the SMWA (groove width: $\approx 50 \mu\text{m}$; groove depth: $\approx 100 \mu\text{m}$) with a period of $\approx 150 \mu\text{m}$ and an oblique angle of $\approx 45^\circ$ which are both finely tunable (period: 30–200 μm , oblique angle: 30–90°). It is observed that nanoscale textures exist on the slant wall structure (the panels on the top in Figure 1b), which can promote the superhydrophobic ability with an apparent contact angle of $\approx 156^\circ$. We define three directions: X (along the slant direction of the SMWA), Y (along the wall direction), and Z (perpendicular to the sample). The droplet can be transported under X-axis vibration while it cannot transport under the other two vibration directions (Figure 1c,e). Along the Y-axis direction, the SMWAs are symmetric, so the droplet undergoes a movement back and forth without transport. Under the Z-axis vibration, the droplet deforms significantly in the vertical direction with no transport. The reason is that during the vertical vibration of the SMWA, the triple contact line at the leading edge of the droplet is not long enough to produce a sufficient pinning force difference due to the excellent superhydrophobicity and lower adhesion of the SMWA.^[30]

To reveal the underlying mechanism of unidirectional microdroplet transport on SMWAs, we recorded the droplet motion with high-speed camera in Video S3, Supporting Information, and established a mechanical analysis model (Figure 2). Figure 2a clarifies the relationship between the displacement and time in the droplet transport process. The top, middle, and bottom panels, respectively, correspond to the half-period (16.5 ms), full-period (33.0 ms), and net displacement of a droplet, in which the period refers to the sinusoidal excitation signal. A positive value indicates that the movement direction is consistent with the slant direction of the microwalls, while a negative value indicates that the movement direction is opposite. The half-period displacement (D_{half}) is a sampling distance based on the half-period of the sinusoidal signal, and the single-period displacement (D_{full}) is a sampling distance based on the full period of the sinusoidal signal (the half-period and single-period displacements are not accumulated, and each sampling

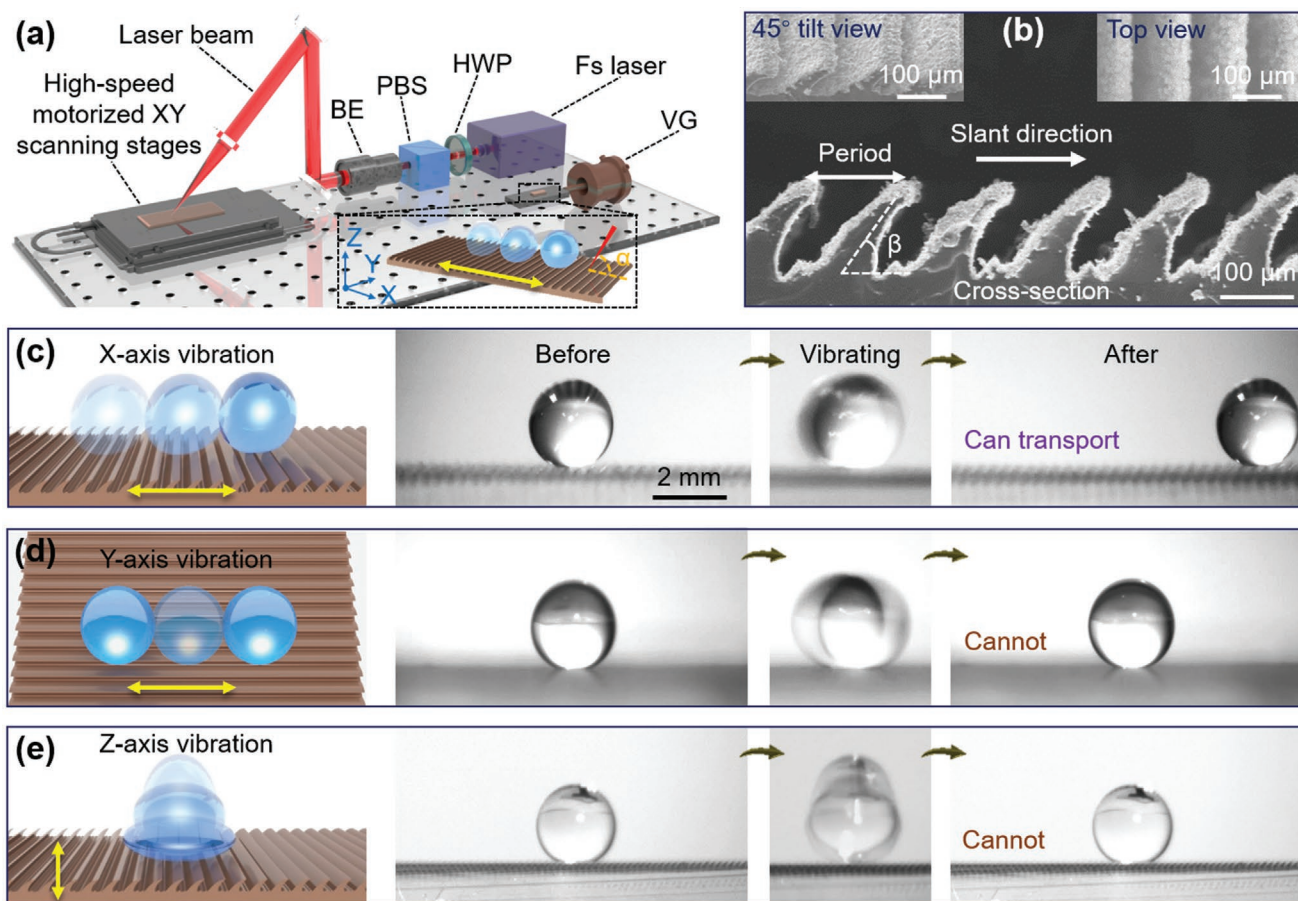


Figure 1. Unidirectional microdroplet transport actuated by horizontal vibration on SMWA fabricated by one-step FLOA. a) Schematics of femtosecond laser oblique ablation (FLOA) apparatus and droplet transport on horizontally vibrating superhydrophobic slant microwall arrays (SMWA) fabricated by one-step FLOA on poly(dimethylsiloxane) (PDMS). The as-fabricated SMWA is mounted on the vibration generator, which can vibrate respectively in three directions: X, Y, and Z. Inclined angle between laser focusing and X-axis is α . BE: beam expander; PBS: polarized beam splitter; HWP: half-wave plate; VG: vibration generator. The yellow arrows represent the vibration direction, which are the same as follows. b) SEM images of the SMWA indicate a period of $\approx 150 \mu\text{m}$ and an oblique angle (β) of $\approx 45^\circ$, which are both finely tunable (period: 30–200 μm , oblique angle: 30–90°). Comparison of droplet motion dynamics when the SMWA is vibrating in three directions respectively. c) Figure shows that droplet transport occurs owing to the asymmetrical superhydrophobic slant microwalls under the X-axis vibration. d) Figure shows that the droplet oscillates in situ left and right due to the symmetrical microstructures under the Y-axis vibration. e) Figure shows that the droplet is extruded and deformed under the Z-axis vibration with no transport because of the insufficient driving force induced by viscous resistance difference even though dewetting is more sensitive to microstructures than wetting.^[30]

is independent from the others). The net displacement (D_{net}) is the displacement of the droplet relative to the initial position, and the sampling interval is a half-period. It is observed that an apparent displacement increase exists in the bottom panel of Figure 2a which corresponds to the three insets indicating the different positions of the droplet. Figure 2b shows droplet movement between 462 and 726 ms in Figure 2a captured by a high-speed camera in Video S4, Supporting Information. The left panel manifests the images with time intervals of ≈ 16.5 ms (half-period) between 462 and 726 ms. The right panel shows the images with time intervals of 2 ms between 462 and 495 ms. It is interesting that the central position of the droplet is connected to fit a curve similar to a sine wave. The reason may be that the displacement of the vibration table is also a sinusoidal type due to the sinusoidal excitation signal.

To clarify the interplay among the inertial forces, interfacial forces, and viscous dissipation forces, we directly calculate

and analyze the relevant dimensionless numbers including the bond number (Bo), capillary number (Ca), and Reynolds number (Re). By substituting the parameters including liquid density $\rho \approx 1 \text{ mg mL}^{-1}$, gravitational acceleration $g \approx 9.8 \text{ m s}^{-2}$, characteristic droplet radius $r \approx 1 \text{ mm}$ and water surface tension $\sigma \approx 0.072 \text{ N m}^{-1}$, the bond number is calculated as $Bo = \rho g r^2 / \sigma \approx 0.136 < 1$. The small Bo indicates that surface tension occupies a dominant role over the gravitational force. So a nearly perfect spherical shape of water droplet can maintain and water will not penetrate into the microgrooved structures to form a Wenzel state. By substituting the dynamical viscosity of water $\mu \approx 1 \text{ mPa s}$, characteristic average velocity of water droplet $v \approx 11.5 \text{ mm s}^{-1}$ and σ , the capillary number, Ca , is calculated as $Ca = \mu v / \sigma \approx 16 \times 10^{-5}$, which is also small enough to manifest that the viscous dissipation is nearly negligible compared with surface tension. Thus, during the transport process of water droplet, the droplet will not deform or spread to form a

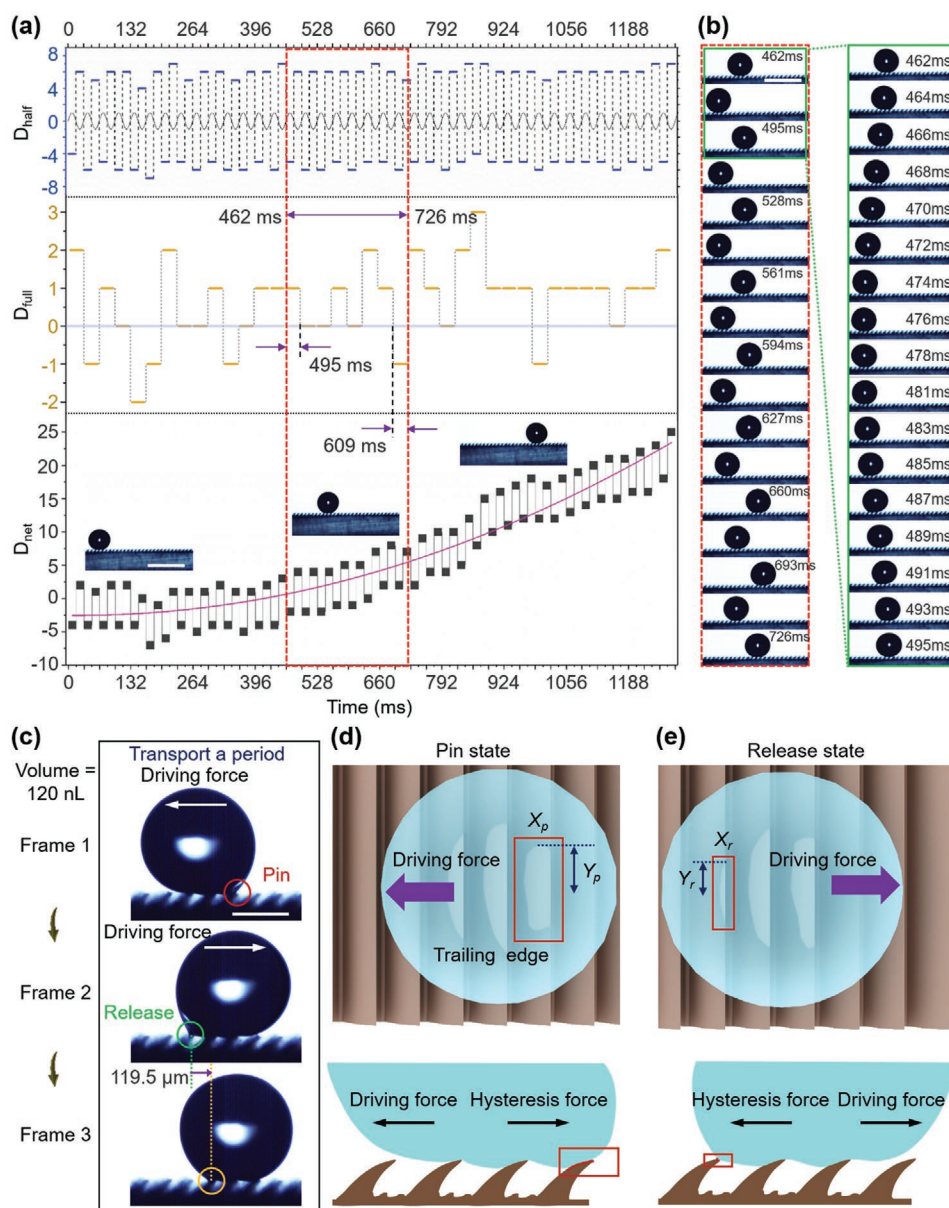


Figure 2. High-speed dynamic process, modeling, and mechanical analysis of microdroplet manipulation on superhydrophobic SMWA. a) The net displacement of the droplet oscillates within short time with a steady increase within longer time in the unidirectional transport process. The upper, middle, and lower panels respectively manifest the half-period (≈ 16.5 ms), full-period (≈ 33 ms), and net displacement of the droplet. The period refers to the sinusoidal excitation signal from a signal generator (top). b) High-speed camera snapshots of droplet transport corresponding to the time period between 462 and 726 ms in (a). The red dotted lines on the left panel indicate the forward or backward distance of droplets in each period, which corresponds to the displacement of 1, 0, 0, 1, 0, 2, 1, and -1 (structural period number of SMWA) within 462–726 ms. The panel on the right shows that the central position of the droplet within 462–495 ms is connected for fitting, which is similar to a sinusoidal shape due to the sinusoidal excitation signal shown in the upper panel of (a). c) High-speed camera snapshots of droplet movement (≈ 120 nL) during a motion period. Frame I (II): The inertial driving force F_{driving} is opposite to (II: the same as) the slant direction of SMWA, which has high (II: low) resistance to the droplet's movement, and there is a critical situation that the trailing edge of the droplet is about to leave but does not (II: does) leave the microwall. Frame III: at the next moment in frame II, the droplet is successfully separated from the microwall and advances one structural period (≈ 119.5 μm). d, e) Modeling and mechanical analysis corresponding to the two critical situations in frame I and II. It is clearly observed that the trailing edge of the droplet in the “Pin” state is larger than that in the “Release” state, which results in a higher viscous resistance.

water film. By constituting ρ , v , r , and μ , the Reynolds number Re is calculated as $Re = 2\rho vr/\mu \approx 23$, which means that droplet transport on SMWA by mechanical vibration is a low-Reynolds-number motion. By analyzing the three dimensionless numbers including Bo , Ca , and Re , the surface tension rather than

gravity or viscous dissipation force plays a dominant role in the analysis of the droplet motion by vibration.

Figure 2c presents three frames of a video showing the motion state of a droplet (≈ 120 nL) under the X-axis vibration during a period of reciprocating motion. Frame I: when the

moving direction of the droplet is opposite to the slant direction of SMWA, the inertial driving force F_{driving} is opposite to the slant direction. The slant wall structure has high resistance force $F_{\text{resistance}}$ to the movement of the droplet, and there is a situation where the receding edge of the droplet is about to leave but has not yet left the microwalls (red circle "Pin"). At this moment, the relationship between driving force and resistance is $F_{\text{driving}} \leq F_{\text{resistance, pin}}$. Frame II: when the microdroplet moves in the same direction as the slant direction of the SMWA, the inertial driving force is along the slant direction. The slant microwall have low resistance to the droplet's movement, and the droplet's hysteresis edge is about to break away from the wall (red circle "Release"). At this moment, the relationship between driving force and resistance is $F_{\text{driving}} \geq F_{\text{resistance, rel}}$. Frame III: at the next moment after frame II, the droplet is successfully separated from the wall and advances one structural cycle ($\approx 120 \mu\text{m}$). Figure 2d,e show mechanical analysis models corresponding to the two critical states in Figure 2c. The droplet in Figure 2d corresponds to the "Pin" state in frame I while the droplet in Figure 2e corresponds to the "Release" state in frame II. The shadow in the red rectangle of the top view is the area where the droplet hysteresis edge touches the slant plate. X_p , Y_p (or X_r , Y_r) are the length and width corresponding to the contact area under the "Pin" (or "Release") states, respectively. So, the resistance force $F_{\text{resistance}}$ can be expressed as:

$$F_{\text{resistance, rel}} \propto X_r Y_r \sin \varphi_r \quad (1)$$

$$F_{\text{resistance, pin}} \propto X_p Y_p \sin \varphi_p \quad (2)$$

where φ denotes the angle between solid-liquid contact line and horizontal direction. Actually, the $F_{\text{resistance, pin}}$ is always larger than the $F_{\text{resistance, rel}}$ due to a larger X and Y , which is the primary reason for unidirectional droplet transport. And φ is almost the same in both cases because of the wall tilted angle of $\approx 45^\circ$. The red line in the red rectangle (the bottom image of Figure 2d,e) also indicates the area where the receding edge is in contact with the slant plate structure. It is clearly observed that the receding edge of the droplet in the state of frame I ("Pin" state) is larger than that of the droplet in contact with the slant plate structure in the state of frame II ("Release" state). Furthermore, the inertial driving force can be expressed as:

$$F_{\text{driving}} = -4\pi^2 m f^2 X_0 \sin(2\pi ft + \varphi_0) \quad (3)$$

where m denotes the mass of the droplet, f denotes the frequency of the excitation signal, X_0 denotes the displacement amplitude of the vibration platform, t denotes the time, φ_0 denotes the initial phase of the excitation signal. The actual maximum inertial driving force is $5.68 \mu\text{N}$ calculated by substituting the experimental data of $m \approx 4 \text{ mg}$ ($4 \mu\text{L}$), $f \approx 30 \text{ Hz}$, and $X_0 \approx 40 \mu\text{m}$. Additionally, the viscous resistances are 3.96 and $7.14 \mu\text{N}$, respectively, along the slant direction and the reverse direction of SMWA in Figure S4, Supporting Information. It is demonstrated that the inertial driving force is between the two viscous resistances, which also accords with the gravity component on inclined SMWA at different tilted angles in Figure S5, Discussion S2.1, Supporting Information. So, there are three situations corresponding to the motion pattern of droplets:

When the equivalent inertial driving force is smaller than the viscous resistance in the both directions:

$$F_{\text{driving}} < F_{\text{resistance, rel}} < F_{\text{resistance, pin}} \quad (4)$$

The droplet cannot move forward or backward and merely oscillates in situ (Video S1, Supporting Information).

When the equivalent inertial driving force is between the two viscous resistance:

$$F_{\text{resistance, rel}} < F_{\text{driving}} < F_{\text{resistance, pin}} \quad (5)$$

The droplet can move forward without moving backward, achieving a rolling motion (Video S2, Supporting Information).

When the equivalent driving force is larger than the two viscous resistances:

$$F_{\text{resistance, rel}} < F_{\text{resistance, pin}} < F_{\text{driving}} \quad (6)$$

The droplet can move forward and backward within a period. But, the forward displacement is greater than the backward displacement, thus achieving a net positive displacement (Figure 2a,b). It is worth mentioning that droplets on the vibrating SMWA maintain the Cassie-like wetting state due to the ultrahigh water-repellency of superhydrophobic micro-grooved array structures,^[31,32] which can be identified by the relatively constant apparent contact angle of droplet deposited on the SMWA during the process of transport in Video S4, Discussion S2.2, Supporting Information.

We explore the effects of key structural parameters of the SMWA on droplet motility and discover four main droplet motion modes under different excitation conditions (Figure 3). Among several structural parameters, the groove width and groove depth have been chosen for optimization because of their controllability, easy tuning, and significant influence on the motion of the droplet in Figure S6, Supporting Information. By increasing n (the number of times for sequential laser scanning within a single groove) from 1 to 9, the groove width (full groove width at half maximum) and groove period (full period at half maximum) can be finely tuned from 29 to $176 \mu\text{m}$ (width) and from 50 to $233 \mu\text{m}$ (period). While varying the above parameters, the groove depth (full depth at half maximum, $114\text{--}126 \mu\text{m}$) and the plate width (full plate width at half maximum, $44\text{--}48 \mu\text{m}$) are almost unchanged, which proves the effectiveness of the single variable control method. Similarly, the groove depth ($52\text{--}188 \mu\text{m}$) can also be tuned precisely by controlling the laser power ($50\text{--}250 \text{ mW}$) with little change to the groove width ($152\text{--}162 \mu\text{m}$), period ($186\text{--}196 \mu\text{m}$) or plate width ($20\text{--}58 \mu\text{m}$) (Figure 3b). To evaluate the droplet manipulation capacity rationally and effectively, we define a parameter K which denotes the sum of the number of effective movements (rolling transport and bouncing transport) in the test of 20 combinations of operating parameters (excitation frequency: $10, 20, 30, 40,$ and 50 Hz ; vibration amplitude: $5, 10, 15,$ and 20 Vpp) in Figures S7 and S8, Supporting Information. It is easily observed that there is an optimal groove width ($\approx 64 \mu\text{m}$) to achieve the best droplet transport capacity ($K = 9$). The reason is that when the groove width is too small, the viscous resistance difference of the SMWA is not enough

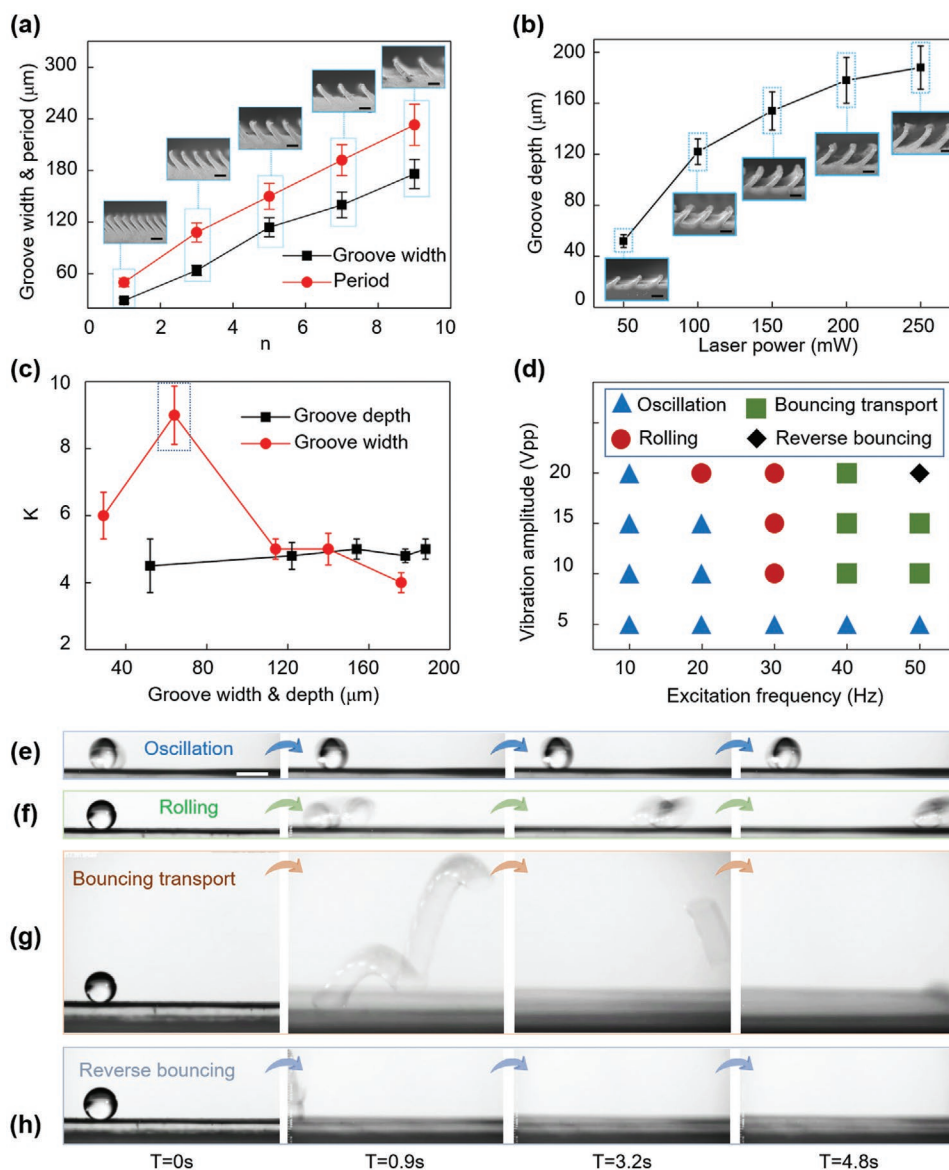


Figure 3. Controlling microdroplet manipulation capacity and modes by designing key structural parameters of the SMWA. a) The groove width (29–176 μm) and groove period (50–233 μm) are increasing with the increase of line-scanning replicates n (1–9) in a single microgroove. b) The groove depth (52–188 μm) is increasing with the increase of the laser power (50–250 mW). c, d) Effects of a single variable (groove width or depth) on droplet motility. There is an optimal groove width ($\approx 64 \mu\text{m}$) enabling the best droplet motility ($K \approx 9$). But there is not obvious change over a large range of groove depth. K is defined as the sum of rolling transport and bouncing transport times that can move correctly in 20 tests shown in (d) (excitation frequency: 10, 20, 30, 40, and 50 Hz; vibration amplitude: 5, 10, 15, and 20 Vpp). e–h) The optical snapshots of different droplet motion modes (in situ oscillation, rolling transport, bouncing transport, and reverse bouncing).

to manipulate the droplet and when the groove width is too large, the energy barrier caused by the gravitational potential energy of the droplet is too large to overcome in Figure S9, Discussion S2.3, Supporting Information. In addition, for different groove depth, K keeps constant because the droplet cannot touch the bottom of the groove. As the amplitude and frequency of the excitation signal increases, the droplet motion experiences four modes in sequence, namely in situ oscillation, rolling transport, bouncing transport, and reverse bouncing. It is speculated that the kinetic energy transferred to the droplet by the vibration platform increases with the increase of signal

amplitude and frequency, and the elastic interaction between the droplet and the SMWA exceeds the effect of viscous resistance, resulting in the change of motion mode (Discussion S2.4, Supporting Information). Figure 3e, h show the selected snapshots captured by the charge coupled device (CCD) presenting four types of droplet motion modes: in situ oscillation of Video S5, Supporting Information, rolling transport of Video S1, Supporting Information, bouncing transport of Video S6, Supporting Information, and reverse bouncing in Figure S10 and Video S7, Supporting Information. The speed of rolling transport is up to 22.86 mm s^{-1} , twice as fast as the average

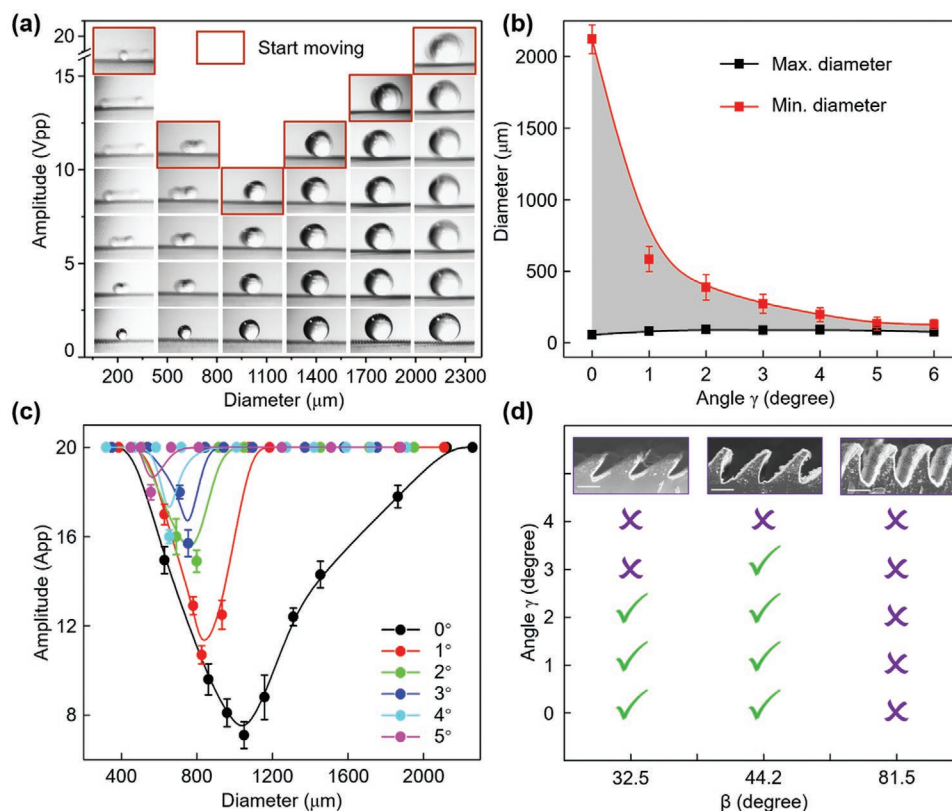


Figure 4. Microdroplet grade-ability on the tilted SMWA controlled by vibration parameters and structural parameters. a) The minimum excitation signal amplitude for droplets of different sizes to start moving. b) The volume ranges of droplets that can be correctly transported decreases with the increase of sample tilt angles. c) The minimum excitation signal amplitude required for droplets of different sizes to move correctly at different sample tilt angles (0–5°). d) The influence of different wall tilted angles (32.5°, 44.2°, and 81.3°) on the grade-ability.

velocity ($\approx 11.5 \text{ mm s}^{-1}$) of the droplet centroid reported in the previous results.^[30] Various modes of motion are expected to be helpful for droplets to move over complex topographies in Figure S11, Supporting Information.

To investigate the impacts of various parameters on the droplet manipulation performance of the SMWA, we have studied the relationship among transport capacity and operation parameters (vibration amplitude), performance parameters (droplet volume and tilted angles of the substrate), and structural parameters (wall tilted angle) (Figure 4). As shown in Figure 4a, droplets of different diameters are placed on vibration platforms with different excitation amplitudes, the red box indicates the start of droplet movement in Video S8, Supporting Information. We can find that too big or too small droplet needs strong excitation amplitude. The smallest microdroplet ($\approx 53 \text{ nL}$) can be actuated because of its rolling motion mode. There is an optimal droplet size ($\approx 0.6 \mu\text{L}$) with which the droplet motion can be actuated by the smallest amplitude (7 Vpp). We further conducted the analysis of the grade-ability of droplets on SMWAs (Figure 4b). Droplets of various diameters are placed on a vibrating SMWA at different sample tilted angles. As the sample tilted angle increases, the controllable volume ranges of the droplets decreases. It is easy to derive that the larger the sample tilted angles, the larger the required excitation amplitudes due to the increased component of gravity (Figure 4c). In addition, the influence of different wall

tilt angles (32.5°, 44.2°, and 81.3°) on the grade-ability of droplets was also studied (Figure 4f), which manifests a possible optimal wall tilted angle of $\approx 45^\circ$.

Additionally, we designed and fabricated a series of circular SMWA, namely CSMWAs in Figure S12, Supporting Information, which have an inside or outside slant direction to achieve the functions of microdroplet convergence and diffusion (Figure 5). The schematic diagrams and pictures captured by CCD show the functions of convergence and diffusion, respectively (Figure 5a,b). The droplets “1,” “2,” and “3” can accumulate on the CSMWA with center-tilted walls while the droplets “4,” “5,” and “6” can diffuse on the CSMWA with outward-tilted walls in several seconds of Videos S9–S12, Supporting Information. A droplet of inappropriate volume ($\approx 0.87 \mu\text{L}$) cannot be actuated because of the symmetry of structures along the vibration direction under the certain excitation conditions. Figure 5c,d present the convergence and diffusion of many small droplets under in-plane horizontal vibration in Videos S13 and S14, Supporting Information. First, the droplets were formed on the sample surface by humidifier or microsyringe. The microdroplets on the CSMWA with center-tilted walls finally converge into several large droplets (Figure 5c) which couldn't be actuated on account of their oversized diameters. But the droplets on the CSMWA with outward-tilted walls could diffuse out of the sample (Figure 5d). The statistical diagrams on the right column of Figure 5c,d show that the number of

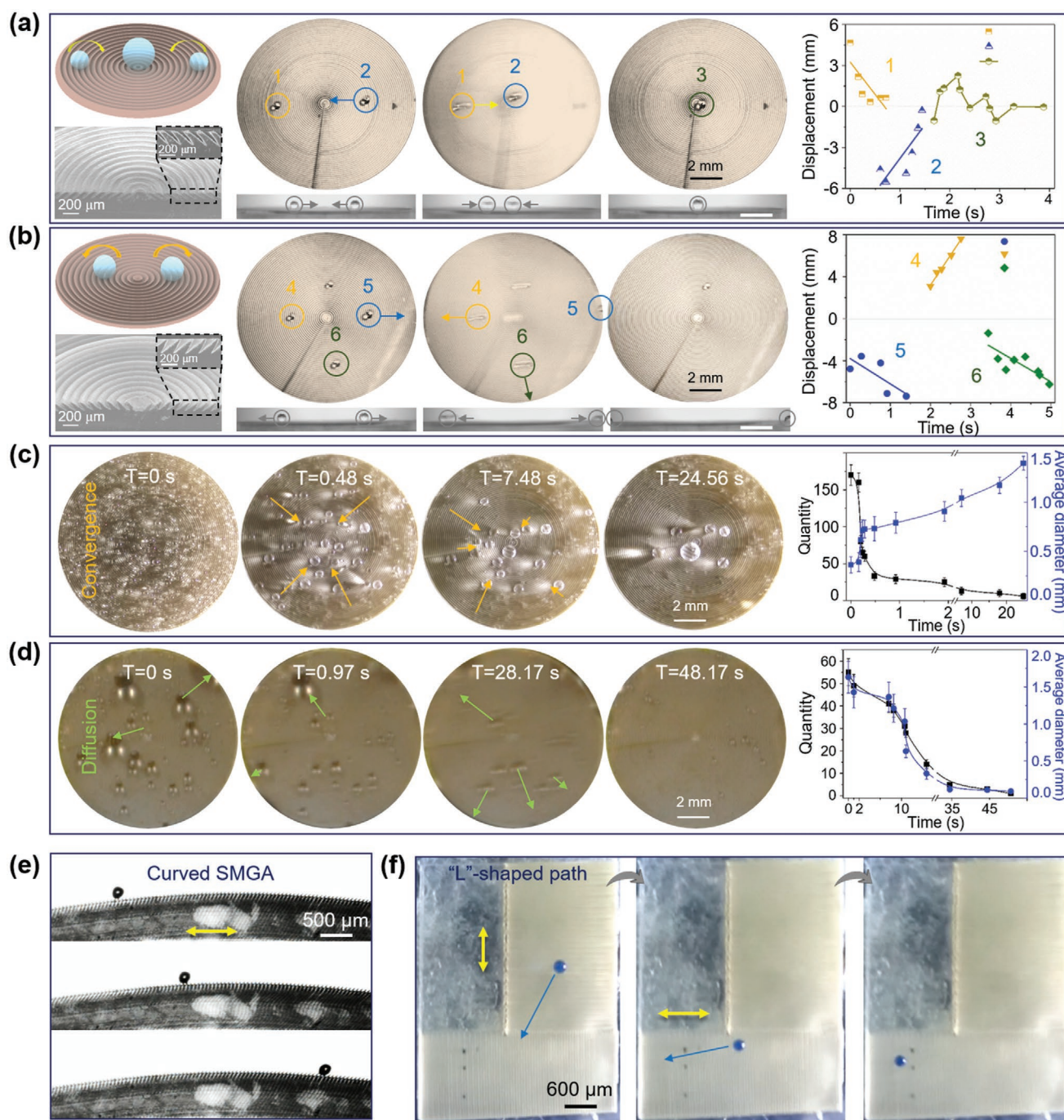


Figure 5. Particular microdroplet motion on the circular, curved and “L”-shaped SMWA actuated by horizontal vibration. a, b) Convergence and diffusion of specific droplets on the inward and outward circular SMWA (CSMWA). Left: schematics and SEM images. Middle: droplet “1” and droplet “2” move inward and converge to form droplet “3,” while droplet “4,” droplet “5,” and droplet “6” move outward and leave out of the CSMWA. Another small droplet stays due to improper size ($\approx 0.87 \mu\text{L}$) and the symmetry of structures along the vibration direction. Right: the displacement of specific droplet versus time. c, d) Convergence and diffusion of plentiful droplets on the inward and outward CSMWA. Left: As the CSMWA vibrates horizontally, droplets on the inward CSMWA gradually converge into several larger droplets in the central area, while droplets on the outward CSMWA diverge out of the sample. There are additionally a few droplets that cannot be transported due to their incorrect volumes. Right: the relationship of the droplet quantity and average diameter versus time. e) The rolling transport of a single water droplet on curved SMWA actuated by horizontal vibration. The main panel corresponds to the big curvature ($\approx 109.6 \text{ m}^{-1}$) of SMWA, while the inset corresponds to the small one ($\approx 69.0 \text{ m}^{-1}$). f) The time-lapse images showing the droplet motion along a “L”-shaped path on the SMWA actuated by the vibration whose direction is varied to match the orientation of the microwalls.

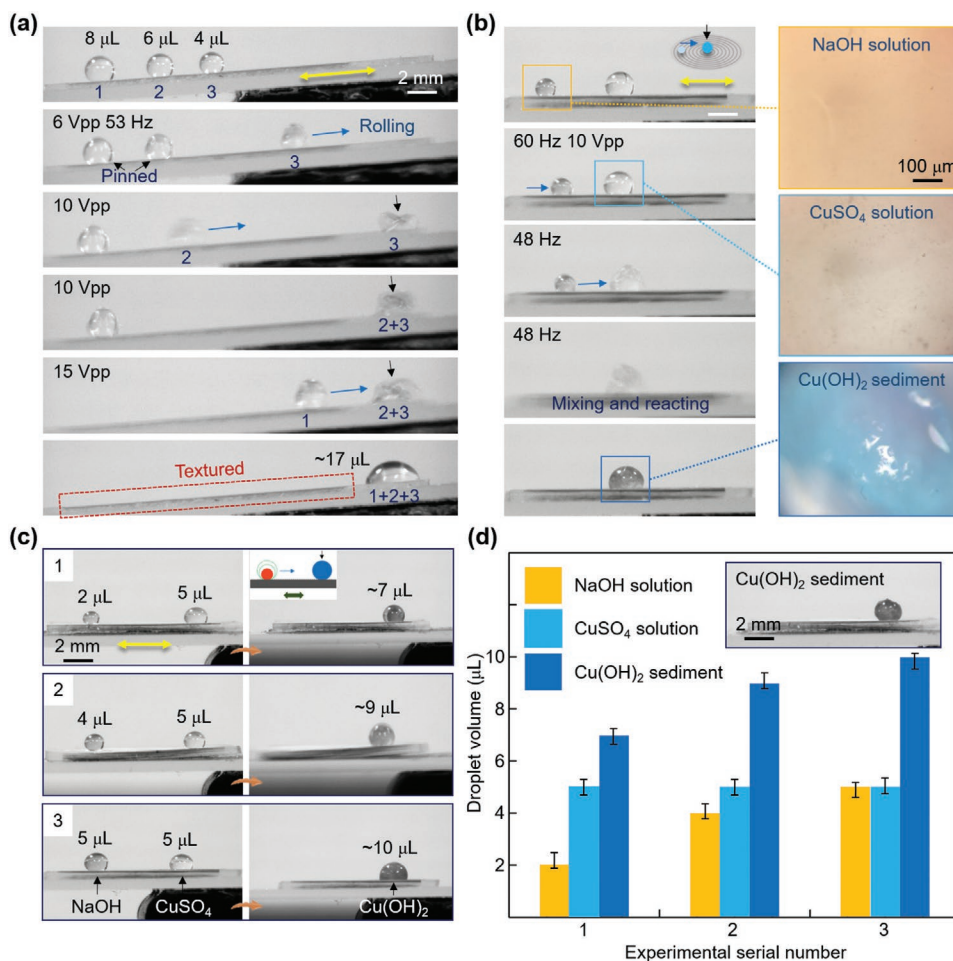


Figure 6. Sequential transport of large-volume-range droplets and chemical mixing microreaction of water-based droplets. a) Sequential droplets transport with different volumes (8, 6, and 4 μL) marked as "1," "2," and "3." Under different excitation amplitudes of 6, 10, 15 Vpp (the same frequency of 53 Hz), the droplet "3" is first actuated with subsequent transport of droplet "2" and "3." The sample was deposited at a slant angle of $\approx 4^\circ$. b) A droplet of NaOH solution (3 μL) is successfully transported to mix with another droplet of CuSO₄ solution (5 μL), which results in a replacement reaction to produce Cu(OH)₂ sediment. The insets showing the different colors of the inside of diverse droplets or sediment on the SMWA surface, which corresponds to different substances including Na⁺, Cu²⁺, and Cu(OH)₂ sediment. c,d) As shown in (c), droplets of NaOH solution with different volumes (2, 4, and 5 μL) and CuSO₄ solution (5 μL) can be mixed and reacted on the SMWA actuated by horizontal vibration under different conditions. (d) shows the changes of droplet volume before and after the mixing. The inset shows the optical images of Cu(OH)₂ sediment after the sufficient mixing and reacting.

droplets decreases but the diameter of droplets increases in the process of convergence, with the opposite effect being observed during the diffusion process. As shown in Figure 5e,f, particular droplet motion on curved SMWA with different curvature in Figure S13, Videos S15 and S16, Supporting Information, and "L"-shaped SMWA in Figure S14 and Video S17, Supporting Information, actuated by horizontal vibration can be achieved, which manifest the high-performance manipulation of droplet movement.

To demonstrate the potential applications of microdroplet transport on horizontally-vibrating SMWA, we designed and conducted two kinds of experiments including the sequential transport of multi-droplets and large-volume-range droplet mixing and reacting (Figure 6). Three water droplets with different volume (4, 6, and 8 μL) were deposited on the inclined SMWA at a climbing angle of $\approx 4^\circ$. The SMWA attached on the vibration generator can vibrate horizontally under the

stimulation of signal generator. When the excitation frequency is fixed at 53 Hz and the excitation amplitude is relatively small (≈ 6 Vpp), the droplet of ≈ 4 μL is actuated to move directionally to the end of the sample. Simultaneously, other two droplets get pinned due to the insufficient driving force resulting from the relatively low excitation amplitude. As the excitation amplitude increases, the other two droplets are actuated successively to merge with the droplet in the front. Finally, the three droplets of different volume are merged in a successive and controllable way (Figure 6a). In addition, we designed and conducted the mixing and reacting experiments of reactant droplets. First, a droplet of NaOH solution is deposited on the edge of the inward CSMWA, while the droplet of CuSO₄ solution is on the center. Then, under the appropriate vibration parameters (10 Vpp and 48 Hz), the NaOH solution droplet was actuated to move inward and merge with the CuSO₄ solution droplet for the production of Cu(OH)₂ sediment. Optical photographs

in the right column correspond to the interior of the solution or sediment, respectively (Figure 6b). Combing the sequential transport of water-based droplets with the controllable droplet microreaction, we proposed a versatile strategy to realize the large-volume-range mixing and reacting of reactant water-based droplets. For instance, NaOH solution droplets with different volume (Figure 6c) can be respectively actuated to merge with CuSO₄ solution droplet for reacting to produce the Cu(OH)₂ sediment (the inset in Figure 6d). Actually, we can reasonably speculate that any water-based solution reactant droplets can be actuated to mix and react in a controllable and quantitative way by horizontally-vibrating SMWA, which has potential applications in multistep quantitative chemical reaction of complex water-based droplets.

In summary, a high-performance microdroplet manipulation strategy including multimode, large volume range and high transport speed was realized on the SMWA actuated by horizontal vibration. It was revealed that the excellent manipulation ability of the SMWA for water droplets is attributed to the rolling motion mode on the superhydrophobic SMWA. The occurrence of droplet transport on anisotropic superhydrophobic SMWA is governed by the difference of viscous resistance caused by the difference of contact areas between the droplet and slant microwalls, as observed by a high-speed camera. It is worth noting that there is an optimal groove width (64 μm) corresponding to the best droplet transport capacity under various excitation amplitudes and frequencies. We also study the effects of droplet volume, substrate tilt angle, and wall tilt angle on droplet mobility. In addition, the function of particular microdroplet motion on the circular, curved, and “L”-shaped SMWA actuated by horizontal vibration is demonstrated. Finally, Sequential transport and microreaction of water-based droplets are achieved for the mixing and reacting of chemical reactants on the SMWA, which manifests the great potentials in the field of microdroplet manipulation.

Experimental Section

Materials: The PDMS (Sylgard 184 Kit, Dow Corning) film was prepared by mixing the prepolymer and crosslinker at a ratio of 10.5:1. After degasification for about 2 h, the mixture was poured on the glass slide placed on the spin coater. The film thickness of PDMS was controlled by the spin coating time and rotation speed. Then, the PDMS was cured on a heating plate for 1 h at 120 °C. Finally, it was cut into pieces (20 × 8 mm²) for femtosecond laser oblique processing.

Slant Microstructure fabrication: The PDMS film was ablated by line-by-line^[33–35] using femtosecond laser oblique scanning, and the processing area was 15 × 7 mm². The laser beam (pulse width: 100fs; repetition rate: 1 kHz; central wavelength: 800 nm) from a one-box regenerative amplified Ti: sapphire femtosecond laser system (Solstice Ace, Spectra-Physics, USA) was utilized for ablation (Discussion S2.5, Supporting Information). The laser beam was guided onto the PDMS film surface placed on a fast scanning electric displacement table through a biconvex lens (*f* = 30 mm) to make the laser beam focus and scan along the X/Y coordinate direction. The scanning spacing between two adjacent lines can be modulated from 10 to 200 μm. The laser power ranged from 50 to 500 mW, and the scanning speed ranged from 1 to 10 mm s⁻¹.

Instrument and Characterization: Scanning electron microscopy graphs were utilized to analyze the surface topography of the laser-induced PDMS film via use of a field-emission scanning electron microscope (JSM-6700F, JEOL, Japan). The apparent contact angles of

the water were measured on the slant microwalls surface with a contact angle system (CA100D, Innuo, China). The volume of the water droplet was set to be 5 μL. The average values were obtained by measuring five droplets at different locations on the same PDMS film. All the contact and rolling angle measurements were conducted under 10% humidity and 20 °C temperature, respectively.

The Vibration Experiments: Powerful mechanical vibrations were generated to actuate the SMWA sample via the use of a vibration generator (2185.00, Frederiksen, Australia). The excitation signal was sent from a signal generator (DG5000, RIGOL, China) in Figure S15 and S17, Supporting Information. Quantitative volume droplets were produced by microsyringe, and smaller droplets were produced by a fog sprayer.

Supporting Information

Supporting Information is available from the Wiley Online Library or from the author.

Acknowledgements

D.W., Z.Z., and Y.Z. contributed equally to this work. This work was supported by National Key Scientific Instrument and Equipment Development Project (No. 61927814), National Natural Science Foundation of China (Nos. 51805508, 51875544, 61805230), National Key R&D Program of China (2017YFB1104303, 2018YFB1105400) and the Fundamental Research Funds for the Central Universities (WK2090090025). The authors acknowledge the Experimental Center of Engineering and Material Sciences at USTC for the fabrication and measuring of samples. This work was partly carried out at the USTC Center for Micro and Nanoscale Research and Fabrication. The authors would also like to thank Zachary J. Smith of the USTC Department of Precision Machinery and Precision Instrumentation for help with language editing.

Conflict of Interest

The authors declare no conflict of interest.

Keywords

anisotropic slant microstructures, horizontal vibrations, liquid microreactions, microdroplet manipulation

Received: July 24, 2020
Revised: September 28, 2020
Published online: October 30, 2020

- [1] Y. Zheng, H. Bai, Z. Huang, X. Tian, F. Q. Nie, Y. Zhao, J. Zhai, L. Jiang, *Nature* **2010**, *463*, 640.
- [2] M. Liu, S. Wang, L. Jiang, *Nat. Rev. Mater.* **2017**, *2*, 17036.
- [3] H. Bai, J. Ju, R. Sun, Y. Chen, Y. Zheng, L. Jiang, *Adv. Mater.* **2011**, *23*, 3708.
- [4] S. K. Cho, H. Moon, C. J. Kim, *J. Microelectromech. Syst.* **2003**, *12*, 70.
- [5] L. F. Cheow, L. Yobas, D. L. Kwong, *Appl. Phys. Lett.* **2007**, *90*, 054107.
- [6] I. Barbulovic-Nad, H. Yang, P. S. Park, A. R. Wheeler, *Lab Chip* **2008**, *8*, 519.

- [7] M. Washizu, *IEEE Trans. Ind. Appl.* **1998**, *34*, 732.
- [8] P. Dubois, G. Marchand, Y. Fouillet, J. Berthier, T. Douki, F. Hassine, S. Gmouh, M. Vaultier, *Anal. Chem.* **2006**, *78*, 4909.
- [9] L. Frenz, A. E. I. Harrak, M. Pauly, S. Begin-Colin, A. D. Griffiths, J. C. Baret, *Angew. Chem., Int. Ed.* **2008**, *47*, 6817.
- [10] U. Lehmann, S. Hadjidj, V. K. Parashar, C. Vandevyver, A. Rida, M. A. M. Gijss, *Sens. Actuators, B* **2006**, *117*, 457.
- [11] H. H. Shen, S. K. Fan, C. J. Kim, *Microfluid. Nanofluid.* **2014**, *16*, 965.
- [12] G. Huang, M. Li, Q. Yang, Y. Li, H. Liu, H. Yang, F. Xu, *ACS Appl. Mater. Interfaces* **2017**, *9*, 1155.
- [13] H. N. Joensson, H. A. Svahn, *Angew. Chem., Int. Ed.* **2012**, *51*, 12176.
- [14] D. R. Link, E. Grasland-Mongrain, A. Duri, F. Sarrazin, Z. Cheng, G. Cristobal, M. Marquez, D. A. Weitz, *Angew. Chem., Int. Ed.* **2006**, *45*, 2556.
- [15] J. R. Dorvee, A. M. Derfus, S. N. Bhatia, M. J. Sailor, *Nat. Mater.* **2004**, *3*, 896.
- [16] J. A. Lv, Y. Liu, J. Wei, E. Chen, L. Qin, Y. Yu, *Nature* **2016**, *537*, 179.
- [17] J. Li, Y. Hou, Y. Liu, C. Hao, M. Li, M. K. Chaudhury, S. Yao, Z. Wang, *Nat. Phys.* **2016**, *12*, 606.
- [18] Q. Sun, D. Wang, Y. Li, J. Zhang, S. Ye, J. Cui, L. Chen, Z. Wang, H. J. Butt, D. Vollmer, X. Deng, *Nat. Mater.* **2019**, *18*, 936.
- [19] L. Qi, Y. Niu, C. Ruck, Y. Zhao, *Lab Chip* **2019**, *19*, 223.
- [20] N. T. Chamakos, G. Karapetsas, A. G. Papathanasiou, *Colloids Surf., A* **2016**, *511*, 180.
- [21] Y. Dong, H. R. Holmes, K. F. Böhringer, *Langmuir* **2017**, *33*, 10745.
- [22] A. Shastry, M. J. Case, K. F. Böhringer, *Langmuir* **2006**, *22*, 6161.
- [23] R. Borcia, I. D. Borcia, M. Bestehorn, *Langmuir* **2014**, *30*, 14113.
- [24] P. Brunet, J. Eggers, R. D. Deegan, *Phys. Rev. Lett.* **2007**, *99*, 144501.
- [25] P. Hao, C. Lv, X. Zhang, Z. Yao, F. He, *Chem. Eng. Sci.* **2011**, *66*, 2118.
- [26] P. Sartori, D. Quagliati, S. Varagnolo, M. Pierno, G. Mistura, F. Magaletti, C. M. Casciola, *New J. Phys.* **2015**, *17*, 113017.
- [27] S. Daniel, M. K. Chaudhury, *Langmuir* **2002**, *18*, 3404.
- [28] S. Daniel, M. K. Chaudhury, P. G. De Gennes, *Langmuir* **2005**, *21*, 4240.
- [29] N. A. Malvadkar, M. J. Hancock, K. Sekeroglu, W. J. Dressick, M. C. Demirel, *Nat. Mater.* **2010**, *9*, 1023.
- [30] T. A. Duncombe, E. Y. Erdem, A. Shastry, R. Baskaran, K. F. Bohringer, *Adv. Mater.* **2012**, *24*, 1545.
- [31] E. Bormashenko, R. Pogreb, G. Whyman, M. Erlich, *Langmuir* **2007**, *23*, 6501.
- [32] E. Bormashenko, R. Pogreb, G. Whyman, M. Erlich, *Langmuir* **2007**, *23*, 12217.
- [33] S. Jiang, Y. Hu, H. Wu, Y. Zhang, Y. Zhang, Y. Wang, Y. Zhang, W. Zhu, J. Li, D. Wu, J. Chu, *Adv. Mater.* **2019**, *31*, 1807507.
- [34] Y. Zhang, Y. Jiao, C. Chen, S. Zhu, C. Li, J. Li, Y. Hu, D. Wu, J. Chu., *Langmuir* **2019**, *35*, 10625.
- [35] Y. Zhang, Y. Jiao, C. Li, C. Chen, J. Li, Y. Hu, D. Wu, J. Chu., *Int. J. Extreme Manuf.* **2020**, *2*.